PCCP

PAPER

View Article Online
View Journal | View Issue

Cite this: *Phys. Chem. Chem. Phys.*, 2016, **18**, 17592

Shock wave and modeling study of the reaction CF_4 (+M) ⇔ CF_3 + F (+M)

Gary Knight,[a] Lars Sölter,[b] Elsa Tellbach[b] and Jürgen Troe*[b]

Received 4th May 2016,
Accepted 7th June 2016

DOI: 10.1039/c6cp03010f

www.rsc.org/pccp

The thermal decomposition of CF_4 (+Ar) → CF_3 + F (+Ar) was studied in shock waves over the temperature range 2000–3000 K varying the bath gas concentration [Ar] between 4×10^{-6} and 9×10^{-5} mol cm^{-3}. It is shown that the reaction corresponds to the intermediate range of the falloff curve. By combination with room temperature data for the reverse reaction CF_3 + F (+He) → CF_4 (+He) and applying unimolecular rate theory, falloff curves over the temperature range 300–6000 K are modeled. A comparison with the reaction system CH_4 (+M) ⇔ CH_3 + H (+M) is made.

1. Introduction

In spite of its importance in plasma etching and in the pyrolysis and oxidation of fluorocarbons, the dissociation/recombination reaction

$$CF_4\ (+M) \rightarrow CF_3 + F\ (+M) \qquad (1)$$

$$CF_3 + F\ (+M) \rightarrow CF_4\ (+M) \qquad (2)$$

has only rarely been investigated. There was a single direct shock tube study[1] of CF_4 dissociation between 2250 and 3100 K in the bath gas M = Ar with [Ar] in the range $(0.4–1.9) \times 10^{-5}$ mol cm^{-3}. Limiting low pressure behavior was postulated with a (pseudo-)first order rate constant of

$$k_1 = [\mathrm{Ar}]\ 6.15 \times 10^{34}\ T^{-4.64} \exp(-61\,600\ \mathrm{K}/T)\ \mathrm{cm^3\ mol^{-1}\ s^{-1}} \qquad (3)$$

The reverse reaction (2) was studied in the bath gas M = He at 295 K as a function of pressure between 0.7 and 7 Torr,[2] showing the approach of a pressure independent limiting high pressure second order rate constant of

$$k_{2,\infty}\ (295\ \mathrm{K}) = 1.2 \times 10^{13}\ \mathrm{cm^3\ mol^{-1}\ s^{-1}} \qquad (4)$$

This result apparently contradicted results from ref. 3, suggesting an increase of k_2 from 0.6 to 3.8×10^{13} cm^3 mol^{-1} s^{-1} when the pressure of the bath gas Ar varied from 2 to 7 Torr.

Since this earlier work, the equilibrium constant for the dissociation/recombination reaction system

$$K_c = k_1/k_2 = ([CF_3][F]/[CF_4])_{eq} \qquad (5)$$

has been established more reliably,[4–6] such that the data of eqn (3) and (4) can be combined and analyzed in terms of unimolecular rate theory. In doing this, one encounters a number of inconsistencies. In particular, one suspects that reaction (1) in ref. 1 has not been studied in the limiting low pressure range of the unimolecular dissociation but in the intermediate range of the falloff curve. This calls for new experiments over a larger range of bath gas concentrations such as performed in the present work. Furthermore, as the falloff curves are predicted to be "very broad",[7] a combination of experiments with theoretical modeling appears unavoidable. The benefit of this combination of experiments and modeling is the representation of dissociation/recombination rate constants over a wide range of conditions. Because of the uncertain location of the experiments along the falloff curves, however, no new information on the thermodynamics of the system can be derived from the kinetics experiments.

An additional aspect of the present study may be of interest. The comparison of results for the CF_4/(CF_3 + F)-system with those for the CH_4/(CH_3 + H)-system should show the effects of replacing the high frequency modes of CH_4 by lower frequency modes of CF_4. Applying unimolecular rate theory one may inspect whether the differences between the systems can be predominantly be attributed to this effect.

2. Experimental technique and results

We investigated the thermal dissociation of CF_4 in the bath gas Ar in incident and in reflected shock waves. Our shock tube had an inner diameter of 9.4 cm, a test section of 4.15 m length, and a high pressure section of 2.80 m length. H_2 was used as the driver gas and shock waves were generated by bursting of a diaphragm between the two sections. Further details of our technique were described before[8–10] and need not to be repeated here. Mixtures of

[a] *Edwards Innovation Centre, Clevedon, BS21 6TH, UK*
[b] *Institut für Physikalische Chemie, Universität Göttingen, Tammannstrasse 6, D-37077 Göttingen, Germany. E-mail: shoff@gwdg.de*

CF_4 (from Linde, 99.9999%) and Ar (from Air Liquide, 99.9999%) were prepared in large mixing vessels before the experiments. Like in ref. 1, the progress of reaction behind the shock waves was followed by recording UV absorption signals of the reaction product CF_2. The latter is formed by the dissociation of the primary dissociation product CF_3. As the dissociation of CF_3 is much more rapid than reaction (1),[11] the dissociation of CF_4 results in the products CF_2 + 2F. In contrast to ref. 1, we worked with highly diluted reaction mixtures. The strong UV absorption of CF_2 at 248 nm (decadic absorption coefficient near 2.3×10^6 cm^2 mol^{-1}, see ref. 9) allowed us to use mixtures of only 500–1500 ppm of CF_4 in Ar. This completely ruled out secondary bimolecular reactions. Our earlier studies of the CF_2 spectrum and its wavelength and temperature dependence[9] allowed us in addition, to confirm the mass balance of one CF_2 formed per one CF_4 decomposed (within ±10 percent due to the uncertainty of the absorption coefficient of CF_2 and some wall adsorption of CF_4 before the experiments, see below). When the mixtures, after decomposition of CF_4 behind incident waves, were further heated behind reflected waves, the thermal decomposition of CF_2 was also observed, confirming results from ref. 11.

Fig. 1 shows the example of a CF_2 absorption-time profile recorded behind a reflected shock. The dissociation is here observed until completion. The final absorption level, with the known absorption coefficient from ref. 9, allows one to control the (minor) extent of CF_4 loss by wall adsorption in the mixing vessel. This is of importance for experiments in which the reaction could not be followed to completion during the available measuring time (about 1 ms in reflected waves because of the arrival of dilution waves and about 80 μs in incident waves because of the arrival of the reflected shock).

There is one further observation which needs to be taken into account as a small correction. At temperatures where CF_4 does not decompose, one observes small absorption steps behind incident and reflected waves. These can be attributed to the UV absorption continuum of CF_4 which~ broadens with increasing temperature and whose long wavelength tail reaches up to the absorption wavelength 248 nm used for CF_2 detection.[12]

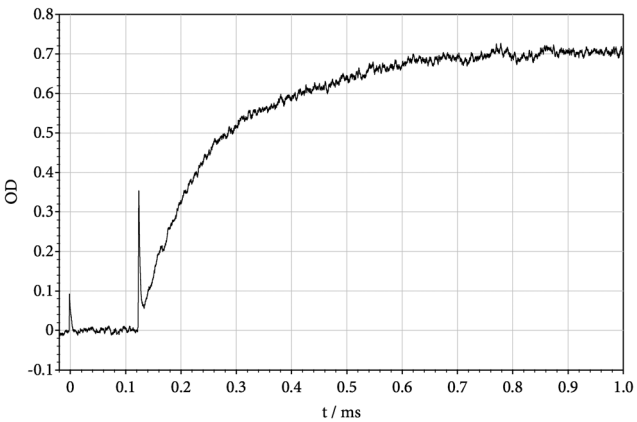

Fig. 1 Absorption-time profile of CF_2 at 248 nm in the dissociation $CF_4 \rightarrow CF_3 + F \rightarrow CF_2 + 2F$ behind a reflected shock wave (T = 2475 K, [Ar] = 6.9×10^{-5} mol cm^{-3}, relative reactant concentration $[CF_4]_{t=0}/[Ar] = 5.3 \times 10^{-4}$).

This observation corresponds to decadic absorption coefficients of CF_4 at 248 nm of $\varepsilon = 6.7 \times 10^4$ cm^2 mol^{-1} at 980 K and $\varepsilon = 9.9 \times 10^4$ cm^2 mol^{-1} at 1890 K. These values are much smaller than those of CF_2 ($\varepsilon = 2.4 \times 10^6$ cm^2 mol^{-1} at 2500 K) such that only small steps at time zero had to be accounted for.

The CF_2 absorption-time profiles strictly followed first order time laws

$$[CF_2] = [CF_4]_{t=0}\{1 - \exp(-k_1 t)\} \quad (6)$$

Table 1 presents values of rate constants k_1/[Ar] together with the experimental conditions. An Arrhenius representation of the values of k_1 is shown in Fig. 2. The data are classified in four groups of Ar concentrations. The high concentration values are apparently systematically lower than the low concentration values. Unfortunately, however, the effect is not large and difficult to characterize quantitatively. Nevertheless, Fig. 2, suggests that the experiments do no correspond to the low pressure limit such as assumed in ref. 1. The modeling presented later on confirms this conclusion. In order to better illustrate the situation, for a temperature of 2500 K Fig. 3 plots the modeled k_1 as a function of [Ar]. As the shown experiments were done at temperatures slightly different from 2500 K, the experimental points were converted to 2500 K with an apparent activation energy of 51 500 K × R as derived from Fig. 2. In spite of the experimental scatter, the data appear fully consistent with the modeled curve obtained later on. Fig. 2 and 3 also include results from ref. 1. There is good agreement between the two experimental studies when data with the same [Ar] are compared. One should note again, however, that the present results were obtained with much lower CF_4 concentrations (0.05–0.15% in the present work *vs.*

Table 1 Experimental conditions (T and [Ar], for relative reactant concentrations of $[CF_4]_{t=0}/[Ar] = 5 \times 10^{-4}$) and rate constants k_1/[Ar] for the decomposition of CF_4

T/K	[Ar]/mol cm^{-3}	k_1/[Ar] cm^3 mol^{-1} s^{-1}
2623	5.0×10^{-6}	4.8×10^8
2632	5.1×10^{-6}	5.0×10^8
2706	4.8×10^{-6}	1.4×10^9
2825	4.4×10^{-6}	2.3×10^9
2907	4.2×10^{-6}	3.8×10^9
3006	4.0×10^{-6}	6.4×10^9
2546	1.4×10^{-5}	2.5×10^8
2081	5.7×10^{-5}	1.5×10^6
2213	5.4×10^{-5}	5.1×10^6
2245	5.2×10^{-5}	1.1×10^7
2343	4.8×10^{-5}	3.5×10^7
2438	4.5×10^{-5}	9.3×10^7
2571	4.1×10^{-5}	2.7×10^8
2717	3.9×10^{-5}	5.2×10^8
2740	5.9×10^{-5}	6.0×10^8
2852	3.7×10^{-5}	1.6×10^9
2935	3.4×10^{-5}	2.7×10^9
2170	9.0×10^{-5}	2.1×10^6
2200	8.4×10^{-5}	5.1×10^6
2260	8.2×10^{-5}	8.5×10^6
2306	7.7×10^{-5}	2.8×10^7
2317	8.0×10^{-5}	3.4×10^7
2353	7.6×10^{-5}	2.1×10^7
2450	7.0×10^{-5}	8.0×10^7
2471	7.0×10^{-5}	1.2×10^8
2475	6.9×10^{-5}	1.0×10^8

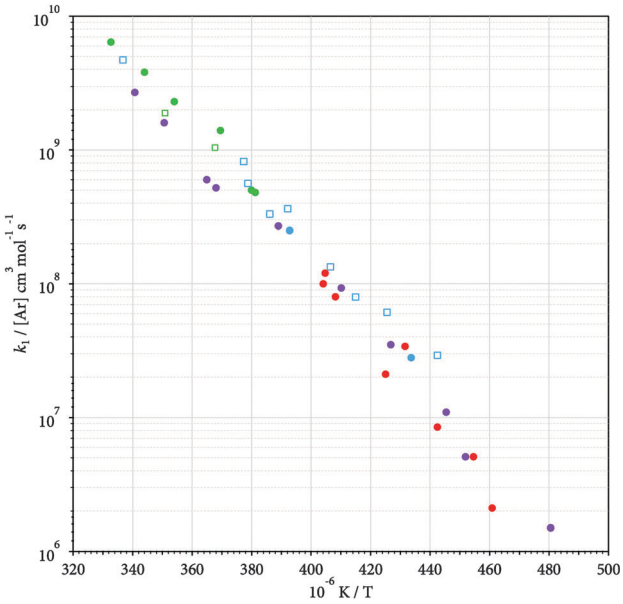

Fig. 2 Rate constants k_1 of the dissociation of CF_4 (results from the present work with [Ar] in 10^{-5} mol cm^{-3}: 6–9: ●, 3–6: ●, 1–2: ●, and 0.4–0.5: ●; results from ref. 1: 0.4–0.5: □, and 1–2: □).

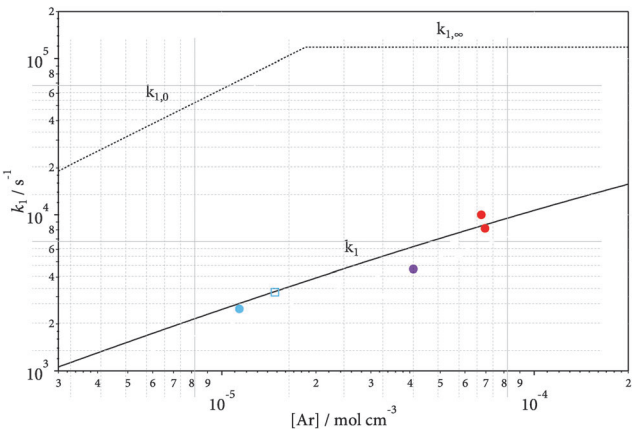

Fig. 3 Rate constants k_1 at T = 2500 K (full line = modeling of this work in comparison to selected experiments from the present work and from ref. 1, see Fig. 2; experimental points converted to 2500 K as described in the text).

1–2% in ref. 1) and with a much broader variation of [Ar] ((0.4–9) × 10^{-5} in the present work *vs.* (0.4–1.9) × 10^{-5} mol cm^{-3} in ref. 1). Furthermore, the small additional contribution from CF_4 absorption was not recognized in ref. 1 (resulting in a 20% increase of the uncorrected rate constants of ref. 1 for the highest temperatures where in contrast to lower temperatures the CF_4 absorption starts to become visible).

3. Modeling of falloff curves

As we expect "broad" falloff curves, *i.e.* falloff curves with center broadening factors F_c smaller than about 0.4, in the present work we used the representation of reduced falloff curves from ref. 7. The falloff curves are expressed in the form

$$k/k_\infty = [x/(1+x)]\,F(x) \tag{7}$$

where k_0 and k_∞ are the respective limiting low and high pressure first order rate constants, $x = k_0/k_\infty$, and $F(x)$ are the broadening factors given by

$$F(x) \approx (1+x)/(1+x^n)^{1/n} \tag{8}$$

with $n = [\ln 2/\ln(2/F_c)]\,(0.8 + 0.2x^q)$ and $q = (F_c - 1)\ln(F_c/10)$ (where ln = $\log_e$). The crucial quantity here is the center broadening factor F_c which is composed of[13,14] a strong collision factor F_c^{sc} and a weak collision factor F_c^{wc}. We estimate the former by the method of ref. 15 while the latter requires an estimate of the collision efficiency β_c, see ref. 13 (β_c later on is derived more precisely from the analysis of k_0). Modeling F_c^{sc} in ref. 15 by RRKM theory requires activated complex frequencies which, for simplicity, here were taken as those[5,6] of CF_4 (omitting 909 cm^{-1} for the reaction coordinate). Modeling F_c^{wc} was done with $\langle\Delta E\rangle/hc \approx -200$ cm^{-1} such as fine-tuned later on. As a first approximation in this way one obtains

$$F_c\ (\mathrm{M = Ar}) \approx 0.12 + 0.88\exp(-T/500\ \mathrm{K}) \tag{9}$$

between 1000 and 3000 K, and

$$F_c\ (\mathrm{M = Ar}) \approx 0.12 + 1.5\exp(-18\,000\ \mathrm{K}/T) \tag{10}$$

between 3000 and 6000 K (F_c (M = Ar) ≈ exp($-T$/100 K) between 300 and 1000 K). F_c = 0.128 (±0.004) is nearly constant between 2000 and 3000 K. This value indeed corresponds to broad reduced falloff curves such that the representation by eqn (7) and (8) is required. As many of the input parameters of a full master equation treatment are not known well enough, such an approach would not appear warranted at this stage and the simplified method of ref. 7 is sufficient.

When $k_{1,\infty}$ can be estimated, the reduced falloff curves allow for a reconstruction of $k_{1,0}$, and hence lead to the full absolute falloff curves k_1 ([Ar], T). At the present stage, $k_{1,\infty}$ is best estimated with the measurements of $k_{2,\infty}$ near 300 K from ref. 2 and the equilibrium constants K_c. $k_{2,\infty}$ from eqn (4) is of similar order of magnitude as the limiting high pressure rate constant for

$$\mathrm{F + CF_2\ (+M) \rightarrow CF_3\ (+M)} \tag{11}$$

which in ref. 16 was determined to be $k_{11,\infty}$ = 2.5 × 10^{13} cm^3 mol^{-1} s^{-1} between 300 and 3000 K. Therefore, it appears safe to assume that $k_{2,\infty}$ is also nearly temperature independent. The comparison with the high pressure rate constant for H + CH_3 (+M) → CH_4 (+M) is also of interest. According to ref. 17, its value of 2.0 × 10^{14} (T/300 K)$^{0.15}$ cm^3 mol^{-1} s^{-1} also has only a weak temperature dependence. Although these reaction systems are of different character, the resulting conclusions on the temperature coefficient of $k_{2,\infty}$ within experimental uncertainty should be adequate. In the following, $k_{2,\infty}$ = 1.2 × 10^{13} cm^3 mol^{-1} s^{-1} from ref. 2 is combined with the equilibrium constant K_c from ref. 5, as represented by

$$K_c = 4.1 \times 10^6\ T^{-1}\exp(-64\,590\ \mathrm{K}/T)\ \mathrm{mol\ cm^{-3}} \tag{12}$$

between 1000 and 6000 K (we emphasize again that the kinetics results do not contribute much to the given K_c; instead K_c here only can be used to link dissociation and recombination rate constants). This leads to a high pressure dissociation rate constant $k_{1,\infty}$ of

$$k_{1,\infty} \approx 4.9 \times 10^{19}\ T^{-1} \exp(-64\,590\ \mathrm{K}/T)\ \mathrm{s}^{-1} \qquad (13)$$

with an estimated uncertainty of about a factor of two. A comparison with the measured rate constants of Table 1 indicates that the present experiments correspond to conditions relatively far from the high pressure range. Combining $k_{1,\infty}$ with modeled reduced falloff curves and comparing the results with the measured k_1 then allows one to reconstruct limiting low pressure rate constants. This is done using k_1 from Fig. 2 (or a tentatively modeled k_1) in order to locate the falloff curves along the pressure axis. Fortunately, the center broadening factors F_c under the present conditions are close to their minimum and practically independent of the conditions. Fitting k_1 from Fig. 2, therefore, without problems leads to the true $k_{1,0}$. Its properties are then further analyzed by unimolecular rate theory in the version of ref. 13. In this analysis there are mainly three contributions which at present stage are difficult to specify, *i.e.* the centrifugal contributions in the rotational factors F_{rot}, anharmonicity contributions expressed by the anharmonicity factor F_{anh}, and the average energy transferred per collision $\langle\Delta E\rangle$ governing the collision efficiency β_c. The centrifugal contributions can be handled with the C–F potential in CF_3, see ref. 11, and were found to be relatively unimportant. That leaves the product $\langle\Delta E\rangle F_{anh}$ to be fitted with the experimental $k_{1,0}$. As this product is expected not to depend strongly on the temperature, one cannot separate it by analysis of falloff curves at different temperatures. However, fitting $\langle\Delta E\rangle\ F_{anh}$ at one temperature and using this value in the theoretically modeled $k_{1,0}$, one can control the result by analyzing falloff curves at different temperatures, here with the experiments near 2000 and 3000 K. Because of the marked shift of the falloff curves along the pressure scale, this is particularly meaningful in the present case. The results are of similar quality as Fig. 3 for 2500 K. We note that we fit a value of the product $\langle\Delta E\rangle F_{anh}/hc$ of about $-560\ \mathrm{cm}^{-1}$. Assuming $\langle\Delta E\rangle/hc \approx -200\ \mathrm{cm}^{-1}$, this corresponds to $F_{anh} \approx 2.8$. Both values appear to be slightly high, but they may include uncertainties from other contributing factors. In any case, the corresponding modeled $k_{1,0}$ can reliably be used for extrapolations to other temperatures. Between 2000 and 6000 K (within a factor of about two) it can be represented in the form

$$k_{1,0} \approx [\mathrm{Ar}]\ 1.5 \times 10^{51}\ T^{-9} \exp(-64\,590\ \mathrm{K}/T)\ \mathrm{cm}^3\ \mathrm{mol}^{-1}\ \mathrm{s}^{-1} \qquad (14)$$

which after conversion with K_c from eqn (12) corresponds to

$$k_{2,0} \approx [\mathrm{Ar}]\ 3.7 \times 10^{44}\ T^{-8}\ \mathrm{cm}^6\ \mathrm{mol}^{-2}\ \mathrm{s}^{-1} \qquad (15)$$

between 2000 and 3000 K (and $k_{2,0} \approx [\mathrm{Ar}]\ 4.7 \times 10^{33}\ T^{-4.7}\ \mathrm{cm}^6\ \mathrm{mol}^{-2}\ \mathrm{s}^{-1}$ between 300 and 2000 K). The marked shift of the falloff curves along the [Ar]-axis most easily is illustrated by plotting k_2 *vs.* [Ar] at different temperatures. This is done in Fig. 4. The experimental results from the present work, after conversion by eqn (12), and the results from ref. 2 for 295 K

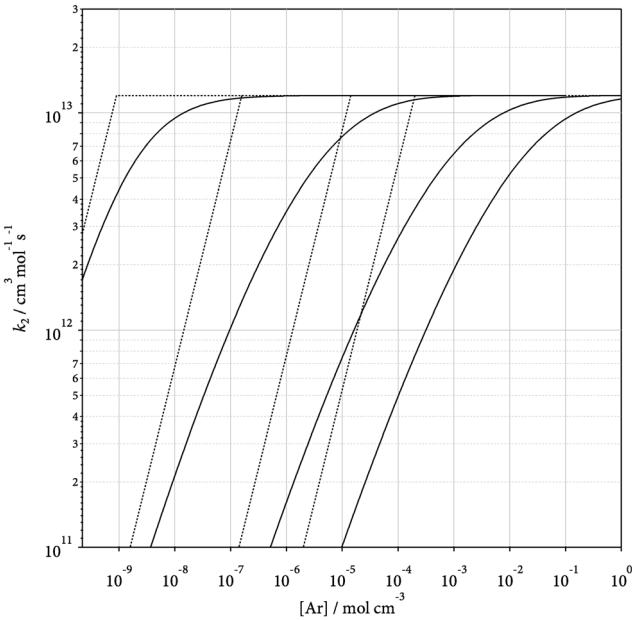

Fig. 4 Modeled falloff curves for k_2, *i.e.* for the recombination F + CF_3 (+Ar) → CF_4 (+Ar) (from left to right for T = 300, 1000, 2000, and 3000 K).

(after accounting for the change of the bath gas to He, with $\langle\Delta E\rangle/hc \approx -20\ \mathrm{cm}^{-1}$) are well represented by these falloff curves. The modeled falloff curve for T = 2500 K in Fig. 3 shows that, because of the experimental scatter, the deviations of the measured k_1 from $k_{1,0}$ could not have been quantified without the modeling.

Comparing falloff curves for the recombination of the CH_4- and CF_4-systems in Fig. 5, one realizes that, at a given temperature, the

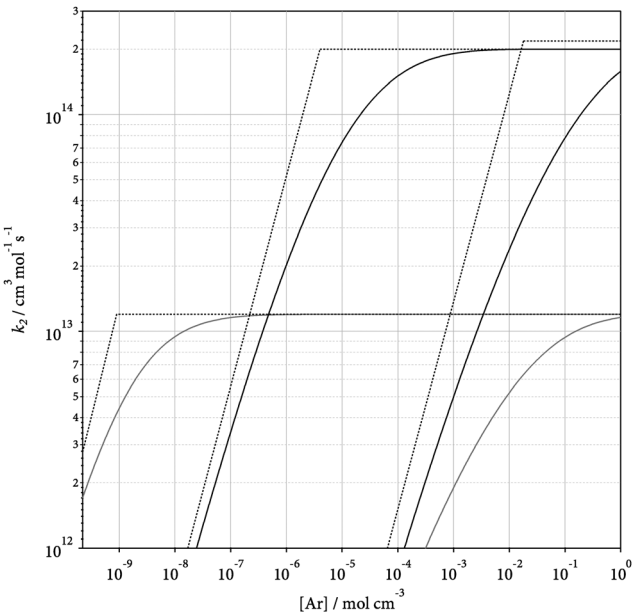

Fig. 5 Comparison of modeled falloff curves for k_2 from this work for F + CF_3 (+Ar) → CF_4 (+Ar) (lower set of curves: data from Fig. 4) and for H + CH_3 (+Ar) → CH_4 (+Ar) (upper pair of curves: data from ref. 17, for T = 300 and 3000 K from left to right).

CF_4-system is closer to the high pressure limit than the CH_4-system. This is attributed to the larger vibrational density of states at the dissociation threshold in CF_4 which arises from the lower fundamental frequencies and the larger dissociation energy and which leads to a larger $k_{1,0}$. The effect in part is compensated by the smaller F_c-values in the CF_4-system and, thus, the broader falloff curves. In addition, however, the larger high pressure recombination rate constant for CH_4 also influences the position of the falloff curves.

4. Conclusions

The present CF_4 dissociation experiments in combination with low temperature recombination data allowed us to provide an internally consistent set of rate constants $k_1([Ar],T)$ and $k_2([Ar],T)$. As the falloff curves of the two reactions were shown to be broad, only the combination of experiments and unimolecular rate theory was able to provide the full picture. The Appendix summarizes the derived rate parameters allowing for a representation of the relevant rate constants over the range 300–6000 K.

Appendix: modeled rate parameters

Temperature range 300–2000 K: $k_{2,0} \approx [Ar]\ 4.7 \times 10^{33}\ T^{-4.7}$ cm^6 mol^{-2} s^{-1} and $k_{2,\infty} \approx 1.2 \times 10^{13}$ cm^3 mol^{-1} s^{-1}.

Temperature range 2000–6000 K: $k_{1,0} \approx [Ar]\ 1.5 \times 10^{51}\ T^{-9} \exp(-64\,590\ K/T)$ cm^3 mol^{-1} s^{-1}, $k_{1,\infty} \approx 4.9 \times 10^{19}\ T^{-1} \exp(-64\,590\ K/T)$ s^{-1}, and $K_c = 4.1 \times 10^6\ T^{-1} \exp(-64\,590\ K/T)$ mol cm^{-3}.

Center broadening factors: F_c (M = Ar) = 0.71, 0.22, 0.13, 0.12, 0.14, and 0.20 for T/K = 300, 1000, 2000, 3000, 4000, and 6000; these results can be represented by F_c (M = Ar) = $\exp(-T/100\ K)$ between 300 and 1000 K, $0.12 + 0.88 \exp(-T/500\ K)$ between 1000 and 3000 K, and $0.12 + 1.5 \exp(-18\,000\ K/T)$ between 3000 and 6000 K.

Broadening factors: it was shown in ref. 7 and 14 that broadening factors $F(x)$ for different reaction systems can be represented in terms of a single parameter F_c only within certain limits, deviating up to about ±10% from eqn (8). However, because of the present small values of F_c, the simpler "standard form" of $F(x)$ from ref. 13 cannot be used here. A comparison of eqn (8) with the large number of alternative propositions cited in ref. 7 remains to be done with respect to their suitability (simplicity and realistic results).

References

1 A. P. Modica and S. J. Sillers, *J. Chem. Phys.*, 1968, **48**, 3283–3289.
2 I. C. Plumb and K. R. Ryan, *Plasma Chem. Plasma Process.*, 1986, **6**, 11–25.
3 N. I. Butkovskaya, M. N. Larichev, I. O. Leipunskii, I. I. Morosov and V. L. Talroze, *Kinet. Katal.*, 1980, **21**, 343–348.
4 V. I. Baranovskii and G. A. Skorobogatov, *Russ. J. Gen. Chem.*, 2016, **86**, 241–250.
5 *J. Phys. Chem. Ref. Data, Monograph No. 9: NIST-JANAF Thermochemical Tables*, ed. M. W. Chase, 4th edn, 1998.
6 A. Burcat and B. Ruscic, *Third Millenium Ideal Gas and Condensed Phase Thermochemical Database for Combustion with Updates from Active Thermochemical Tables*, Argonne National Laboratory, ANL-05/20, Sept. 2005.
7 J. Troe and V. G. Ushakov, *Z. Phys. Chem.*, 2014, **228**, 1–10.
8 C. J. Cobos, K. Hintzer, L. Sölter, E. Tellbach, A. Thaler and J. Troe, *Phys. Chem. Chem. Phys.*, 2015, **17**, 32219–32224.
9 C. J. Cobos, A. E. Croce, K. Luther, L. Sölter, E. Tellbach and J. Troe, *J. Phys. Chem. A*, 2013, **117**, 11420–11429.
10 C. Kappel, K. Luther and J. Troe, *Phys. Chem. Chem. Phys.*, 2002, **4**, 4392–4398.
11 C. J. Cobos, A. E. Croce, K. Luther and J. Troe, *J. Phys. Chem. A*, 2010, **114**, 4755–4761.
12 G. Bélanger, P. Sauvageau and C. Sandorfy, *Chem. Phys. Lett.*, 1969, **3**, 649–651.
13 J. Troe, *J. Phys. Chem.*, 1979, **83**, 114–126.
14 V. G. Ushakov and J. Troe, *J. Chem. Phys.*, 2011, **135**, 054304.
15 J. Troe, *Ber. Bunsen-Ges. Phys. Chem.*, 1983, **87**, 161–169.
16 N. K. Srinivasan, M.-C. Su, J. V. Michael, A. W. Jasper, S. J. Klippenstein and L. B. Harding, *J. Phys. Chem. A*, 2008, **112**, 31–37.
17 J. Troe and V. G. Ushakov, *J. Chem. Phys.*, 2012, **136**, 214309.

